Progress In Electromagnetics Research B, Vol. 17, 213–231, 2009

DIMENSIONAL SYNTHESIS FOR WIDE-BAND BANDPASS FILTERS WITH QUARTER-WAVELENGTH RESONATORS

Q. Zhang and Y. Lu

School of Electrical and Electronics Engineering
Nanyang Technological University
Singapore 639798, Singapore

Abstract—This paper presents a dimensional synthesis method for designing wide-band quarter-wavelength resonator bandpass filters. In this synthesis method, an alternative lowpass prototype filter and the edge frequency mapping method are proposed and applied. The improved K- and J-inverter model with the exponent-weighted turns ratio is also proposed in order to incorporate the frequency dependence of inverters. Based on the edge frequency mapping method and the improved inverter model, an iterative dimensional synthesis procedure is then presented. As design examples, a four-pole rectangular coaxial bandpass filter with 63% fractional bandwidth is designed and fabricated. The simulation and measurement results show good equal ripple performance in the passband.

1. INTRODUCTION

Design techniques for wide-band bandpass filters without excessive global optimization have become more and more important. With the improvement of these techniques, the accuracy, time, and complexity of the design procedure can be improved significantly. And the excessive use of optimization can be avoided especially in complicated structures where there are numerous dimensions to be optimized.

In the classic bandpass filter theories [1], the network with immittance inverters is employed. By using impedance or admittance inverters, microwave bandpass filters can be designed conveniently. However, the inverters have to be frequency-independent theoritically, which is not true for practical cases. One of the most serious degradations in frequency response of a bandpass filter from the ideal

Corresponding author: Q. Zhang (e070022@ntu.edu.sg).

one is due to the frequency sensitivity of the inverters. The general design procedure for direct-coupled filters was first devised by Cohn [4]. And then Matthaei, Young and Jones [1] introduced a bandwidth contraction factor and a deviation of center frequency for direct-coupled cavity filters to predict the change caused by the frequency-dependent inverters using design graphs. Levy, [3], suggested "ideal transformers with frequency-dependent turns ratio" on both sides of the inverters.

These techniques discussed above are employed to design bandpass filters with half-wavelength resonators which, however, have the disadvantage of spurious response below $2f_0$ (twice of the passband frequency). Comparatively, bandpass filters with quarter-wavelength resonators have advantages that the length of the filter is shorter and the second passband center is at $3f_0$ instead of $2f_0$ [5]. So far, however, quarter-wavelength resonator bandpass filters are designed according to the classic method in [5] and no improved synthesis method was reported.

In this paper, we propose a dimensional synthesis method for designing wide-band bandpass filters with quarter-wavelength resonators without global optimization. It is realized in rectangular coaxial structures, which have the advantage of low dielectric loss, low radiation loss and weak cross coupling with other circuits in a system [6]. As design examples, rectangular coaxial bandpass filters are designed using the proposed synthesis method, and the results show good equal ripple performance in the passband.

2. THEORY

2.1. Alternative Lowpass Prototype Filter

Immittance inverters have the ability to shift impedance or admittance levels depending on the choice of K or J parameters. Making use of these properties enables us to convert a filter circuit to an equivalent form that would be more convenient for implementation with microwave structures. Fig. 1 shows the classic lowpass prototype

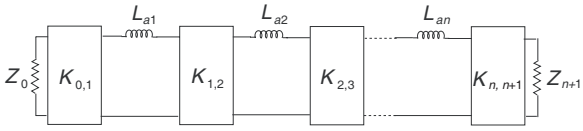

Figure 1. The classic lowpass prototype filter with impedance inverters.

filters with impedance inverters and the K parameters can be calculated as in [1] and [2]:

$$\begin{cases} K_{0,1} = \sqrt{\dfrac{Z_0 L_{a1}}{g_0 g_1}} \\ K_{i,i+1} = \sqrt{\dfrac{L_{ai} L_{a(i+1)}}{g_i g_{i+1}}}\Big|_{i=1,2,\ldots,n-1} \\ K_{n,n+1} = \sqrt{\dfrac{L_{an} Z_{n+1}}{g_n g_{n+1}}} \end{cases}, \tag{1}$$

where the g_i are the normalized elements of the lumped-element lowpass prototype filter [1]. The element values Z_0, Z_{n+1} and L_{ai} in Fig. 1 may be chosen arbitrarily and the filter response will be identical to that of the original prototype, provided that the K parameters are specified as indicated in (1). However, the lowpass prototype filters in Fig. 1 have only K inverters and thus it can be only transformed into bandpass filters with half-wavelength resonators. So we should propose an alternative lowpass prototype filter with alternating impedance inverters and admittance inverters, which can be transformed into bandpass filters with quarter-wavelength resonators.

The impedance inverter with series inductance can be equivalent to an admittance inverter with parallel capacitance and two ideal inverter added on both sides as shown in Fig. 2. The transfer matrix of the ideal inverter is given by

$$\begin{bmatrix} 0 & jZ_0 \\ \frac{j}{Z_0} & 0 \end{bmatrix}, \tag{2}$$

where Z_0 is the input terminating impedance in Fig. 1. The transfer matrix of the left side of Fig. 2 is

$$\begin{bmatrix} 0 & jK \\ \frac{j}{K} & 0 \end{bmatrix} \begin{bmatrix} 1 & j\omega L \\ 0 & 1 \end{bmatrix} = \begin{bmatrix} 0 & jK \\ \frac{j}{K} & -\frac{\omega L}{K} \end{bmatrix}, \tag{3}$$

and transfer matrix of the right side is

$$\begin{bmatrix} 0 & jZ_0 \\ \frac{j}{Z_0} & 0 \end{bmatrix} \begin{bmatrix} 0 & \frac{j}{J} \\ jJ & 0 \end{bmatrix} \begin{bmatrix} 1 & 0 \\ j\omega C & 1 \end{bmatrix} \begin{bmatrix} 0 & jZ_0 \\ \frac{j}{Z_0} & 0 \end{bmatrix} = \begin{bmatrix} 0 & -jZ_0^2 J \\ -\frac{j}{Z_0^2 J} & \frac{\omega C}{J} \end{bmatrix}. \tag{4}$$

To make (3) equivalent to (4), the following condition should be satisfied:

$$\begin{cases} \frac{K}{Z_0} = -\frac{J}{Y_0} \\ \frac{L}{Z_0} = \frac{C}{Y_0} \end{cases}, \tag{5}$$

where $Y_0 = 1/Z_0$.

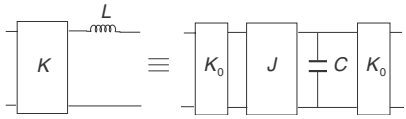

Figure 2. The equivalence of two inverter networks.

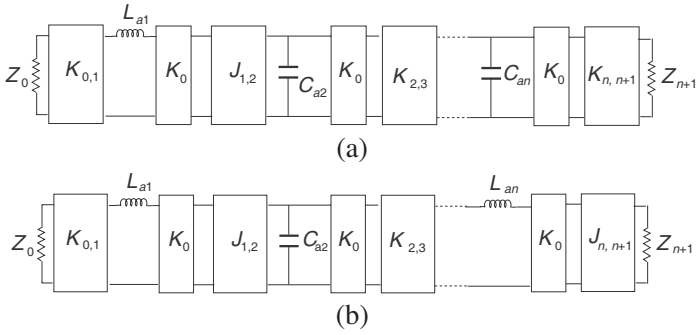

Figure 3. Alternative lowpass prototype filters: (a) n is even, (b) n is odd.

According the equivalence introduced above, we can replace the even number impedance inverters of the lowpass prototype filter in Fig. 1 by the admittance inverters and obtain the alternative lowpass prototype filters as shown in Fig. 3. By substituting (1) with (5), the K parameters and J parameters in Fig. 3 can be expressed as

$$\begin{cases} \frac{K_{0,1}}{Z_0} = \sqrt{\frac{L_{a1}}{Z_0 g_0 g_1}} \\ \frac{K_{i,i+1}}{Z_0} = \sqrt{\frac{C_{ai} L_{a(i+1)}}{g_i g_{i+1}}} \,|_{i=2,4,6,\ldots}\,, \quad \frac{J_{i,i+1}}{Y_0} = \sqrt{\frac{L_{ai} C_{a(i+1)}}{g_i g_{i+1}}} \,|_{i=1,3,5,\ldots} \\ \frac{K_{n,n+1}}{Z_0} = \sqrt{\frac{C_{an} Z_{n+1}}{g_n g_{n+1}}} \,|_{n \text{ is even}}\,, \frac{J_{n,n+1}}{Y_0} = \frac{1}{Z_0}\sqrt{\frac{L_{an} Z_{n+1}}{g_n g_{n+1}}} \,|_{n \text{ is odd}} \end{cases} . \quad (6)$$

Here we only discuss the cases that the first inverter is the impedance inverter and the other two cases that the first inverter is the admittance inverter can be derived in a similar way.

2.2. Equivalent Network for the Quarter-wavelength Bandpass Filter

Figure 4 shows the classic quarter-wavelength resonator bandpass filter, which have alternating high and low impedance levels on two ends of the quarter-wavelength transmission lines [5]. Here we only discussed the case that the first inverter is impedance inverter and the resonator number is even. Other cases can be derived in a similar way.

In order to derive the equivalent network for the quarter-wavelength resonator bandpass filter, we should first derive the equivalent network for the quarter-wavelength transmission line, which has been discussed in [5]. As shown in Fig. 5, the input impedance can be expressed as

$$Z_{in} = Z_0 \cdot \frac{Z_L + jZ_0 \tan \frac{\pi\Omega}{2\Omega_0}}{Z_0 + jZ_L \tan \frac{\pi\Omega}{2\Omega_0}}. \tag{7}$$

If $|Z_L| \gg Z_0$, Equation (7) can be approximated by

$$Z_{in} = Z_0 \cdot \frac{Z_L + jZ_0 \tan \frac{\pi\Omega}{2\Omega_0}}{jZ_L \tan \frac{\pi\Omega}{2\Omega_0}} = jX(\Omega) + \frac{Z_0^2}{Z_L}. \tag{8}$$

According to (8), the equivalent network can be shown in Fig. 5(a) and the series reactance is

$$X(\Omega) = -Z_0 \cot \frac{\pi\Omega}{2\Omega_0}. \tag{9}$$

If $|Z_L| \ll Z_0$, Equation (7) can be approximated by

$$Z_{in} = Z_0 \cdot \frac{jZ_0 \tan \frac{\pi\Omega}{2\Omega_0}}{Z_0 + jZ_L \tan \frac{\pi\Omega}{2\Omega_0}} = \frac{1}{jB(\Omega) + \frac{Z_L}{Z_0^2}}. \tag{10}$$

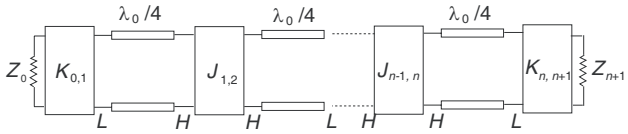

Figure 4. The bandpass filter with quarter-wavelength resonators (n is even).

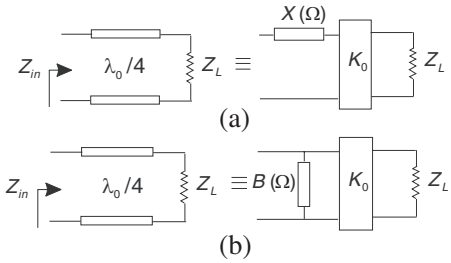

Figure 5. Equivalent network for the quarter-wavelength transmission line: (a) $Z_L \gg Z_0$, (b) $Z_L \ll Z_0$.

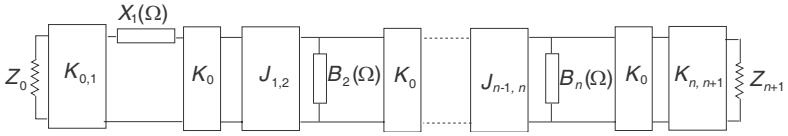

Figure 6. Equivalent network for the quarter-wavelength resonator bandpass filter.

According to (10), the equivalent network can be shown in Fig. 5(b) and the shunt susceptance is

$$B(\Omega) = -Y_0 \cot \frac{\pi\Omega}{2\Omega_0}. \tag{11}$$

By applying the equivalent network in Fig. 5, we can easily derive the equivalent network for the quarter-wavelength resonator bandpass filter as shown in Fig. 6.

2.3. Edge Frequency Mapping Method

Since the lowpass prototype filter in Fig. 3(a) and the equivalent network for the quarter-wavelength resonator bandpass filter in Fig. 6 have been obtained, the transformation from the lowpass filter to the bandpass filter can be derived. Comparing the two networks, we can get the mapping function

$$f : \begin{cases} \omega L_{ai} \to X_i(\Omega), & i = 1, 3, \ldots, n-1 \\ \omega C_{ai} \to B_i(\Omega), & i = 2, 4, \ldots, n \end{cases} . \tag{12}$$

The following condition should be imposed:

$$\begin{cases} X_i(\Omega_0) = 0, \quad B_i(\Omega_0) = 0 \\ X_i(\Omega_1) = -\omega_1 L_{ai}, \quad B_i(\Omega_1) = -\omega_1 C_{ai} \\ X_i(\Omega_2) = \omega_1 L_{ai}, \quad B_i(\Omega_2) = \omega_1 C_{ai} \end{cases} . \tag{13}$$

where ω_1 is the cutoff angular frequency of the lowpass filter, and Ω_0, Ω_1, Ω_2 denote the center angular frequency, lower and upper edge angular frequency of the bandpass filter, respectively. By solving (12) and (13), we can get

$$\begin{cases} L_{ai} = -X_i(\Omega_1)/\omega_1 & i = \text{odd} \\ C_{ai} = -B_i(\Omega_1)/\omega_1 & i = \text{even} \end{cases} , \tag{14}$$

$$\begin{cases} X_i(\Omega_1) + X_i(\Omega_2) = 0 & i = \text{odd} \\ B_i(\Omega_1) + B_i(\Omega_2) = 0 & i = \text{even} \end{cases} . \tag{15}$$

Equation (15) denotes the condition imposed on the center frequency, lower and upper frequency of the bandpass filter. By substituting (6) with (14), the K parameters and J parameters can be calculated.

If the K-inverters and J-inverters in Fig. 6 are considered as ideal inverters, we can get a simple case. By substituting (14) and (15) with (9) and (11), we can get

$$\begin{cases} \frac{L_{ai}}{Z_0} = \frac{C_{ai}}{Y_0} = \frac{1}{\omega_1} \cdot \cot \frac{\pi\Omega_1}{2\Omega_0} \\ \cot \frac{\pi\Omega_1}{2\Omega_0} + \cot \frac{\pi\Omega_2}{2\Omega_0} = 0 \end{cases} . \tag{16}$$

It is noted from (16) that the edge frequency mapping method employs the resonator information both at the center frequency and edge frequency, which is different from the classic mapping method [1] in which the resonator reactance value and the slope parameter at the center frequency are considered.

2.4. Frequency-dependent Inverter Model

The result in (16) is calculated on the condition that all the inverters are ideal; however, the practical inverters are all frequency-dependent. So we present a frequency-dependent inverter model here, which is based on the "turns ratio" concept in [3]. However, the turns ratio we propose here has a more general definition and we also bring in the weight exponent in the decomposition of the inverter. The turns ratio here is defined as

$$m_{i,i+1}(\Omega) = \begin{cases} K_{i,i+1}(\Omega)/K_{i,i+1}(\Omega_0),\ i = 0, 2, \ldots, n \\ J_{i,i+1}(\Omega)/J_{i,i+1}(\Omega_0),\ i = 1, 3, \ldots, n-1 \end{cases} . \tag{17}$$

It is noted from Fig. 6 that there is an ideal inverter on the left side of every frequency-dependent inverter. So we consider them together. The transfer matrix of the frequency-dependent K-inverter together with the ideal inverter on the left can be presented as

$$\begin{aligned} &\begin{bmatrix} 0 & jZ_0 \\ \frac{j}{Z_0} & 0 \end{bmatrix} \begin{bmatrix} 0 & jK_{i,i+1}(\Omega) \\ \frac{j}{K_{i,i+1}(\Omega)} & 0 \end{bmatrix} = \begin{bmatrix} -\frac{Z_0}{K_{i,i+1}(\Omega)} & 0 \\ 0 & -\frac{K_{i,i+1}(\Omega)}{Z_0} \end{bmatrix} \\ = &\begin{bmatrix} m_{i,i+1}^{-i/n}(\Omega) & 0 \\ 0 & m_{i,i+1}^{i/n}(\Omega) \end{bmatrix} \begin{bmatrix} -\frac{Z_0}{K_{i,i+1}(\Omega_0)} & 0 \\ 0 & -\frac{K_{i,i+1}(\Omega_0)}{Z_0} \end{bmatrix} \\ &\begin{bmatrix} m_{i,i+1}^{i/n-1}(\Omega) & 0 \\ 0 & m_{i,i+1}^{1-i/n}(\Omega) \end{bmatrix} . \end{aligned} \tag{18}$$

According to (18), the decomposition for the K-inverter is shown in Fig. 7. It can be seen that the transformer is added only on one

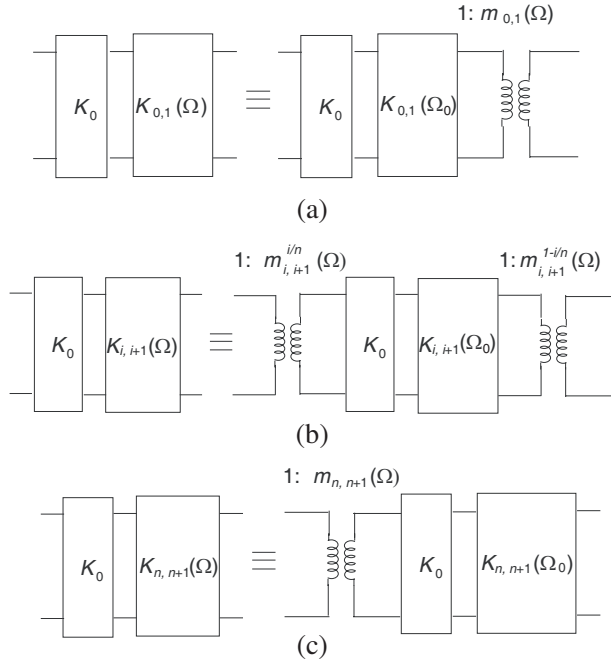

Figure 7. Decomposition of the frequency-dependent K inverters. (a) The first inverter, (b) The $(i+1)$th inverter, (c) The last inverter.

side for the first and last inverter by using the weight exponent. So the frequency dependence of the two end inverters can be distributed equally to all the others. Similarly, the transfer matrix of the frequency-dependent J-inverter together with the ideal inverter on the left can be presented as

$$\begin{bmatrix} 0 & jZ_0 \\ \frac{j}{Z_0} & 0 \end{bmatrix} \begin{bmatrix} 0 & \frac{j}{J_{i,i+1}(\Omega)} \\ jJ_{i,i+1}(\Omega) & 0 \end{bmatrix} = \begin{bmatrix} -Z_0 J_{i,i+1}(\Omega) & 0 \\ 0 & -\frac{1}{Z_0 J_{i,i+1}(\Omega)} \end{bmatrix}$$
$$= \begin{bmatrix} m_{i,i+1}^{i/n}(\Omega) & 0 \\ 0 & m_{i,i+1}^{-i/n}(\Omega) \end{bmatrix} \begin{bmatrix} -Z_0 J_{i,i+1}(\Omega) & 0 \\ 0 & -\frac{1}{Z_0 J_{i,i+1}(\Omega)} \end{bmatrix}$$
$$\begin{bmatrix} m_{i,i+1}^{1-i/n}(\Omega) & 0 \\ 0 & m_{i,i+1}^{i/n-1}(\Omega) \end{bmatrix}. \tag{19}$$

The decomposition of the frequency-dependent J inverter is shown in Fig. 8. The turns ratio can be absorbed by the adjacent distributed resonator elements. Fig. 9 shows the turns ratio absorbed by the series

reactance. The transfer matrix of the new resonator elements is given by

$$\begin{bmatrix} m_{i-1,i}^{(i-1)/n-1}(\Omega) & 0 \\ 0 & m_{i-1,i}^{1-(i-1)/n}(\Omega) \end{bmatrix} \begin{bmatrix} 1 & jX_i(\Omega) \\ 0 & 1 \end{bmatrix} \begin{bmatrix} m_{i,i+1}^{i/n}(\Omega) & 0 \\ 0 & m_{i,i+1}^{-i/n}(\Omega) \end{bmatrix}$$
$$= \begin{bmatrix} m_{i-1,i}^{(i-1)/n-1}(\Omega) \cdot m_{i,i+1}^{i/n}(\Omega) & j \cdot m_{i-1,i}^{(i-1)/n-1}(\Omega) \cdot m_{i,i+1}^{-i/n}(\Omega) \cdot X_i(\Omega) \\ 0 & m_{i-1,i}^{1-(i-1)/n}(\Omega) \cdot m_{i,i+1}^{-i/n}(\Omega) \end{bmatrix}. \quad (20)$$

Since the turns ratio m is very close to 1, the following approximation can be made:

$$m_{i-1,i}^{(i-1)/n-1}(\Omega) \cdot m_{i,i+1}^{i/n}(\Omega) \approx 1. \quad (21)$$

So the new distributed resonator elements can be also regarded as a series reactance. By applying (9), it is expressed as

$$\begin{aligned} X_i^*(\Omega) &= m_{i-1,i}^{(i-1)/n-1}(\Omega) \cdot m_{i,i+1}^{-i/n}(\Omega) \cdot X_i(\Omega) \\ &= -Z_0 m_{i-1,i}^{(i-1)/n-1}(\Omega) m_{i,i+1}^{-i/n}(\Omega) \cot\left(\frac{\pi\Omega}{2\Omega_0}\right). \end{aligned} \quad (22)$$

Similarly, we can derive the turns ratio absorbed by the shunt susceptance as shown in Fig. 10 and the new shunt susceptance can be expressed as

$$\begin{aligned} B_i^*(\Omega) &= m_{i-1,i}^{(i-1)/n-1}(\Omega) \cdot m_{i,i+1}^{-i/n}(\Omega) \cdot B_i(\Omega) \\ &= -Y_0 m_{i-1,i}^{(i-1)/n-1}(\Omega) m_{i,i+1}^{-i/n}(\Omega) \cot\left(\frac{\pi\Omega}{2\Omega_0}\right). \end{aligned} \quad (23)$$

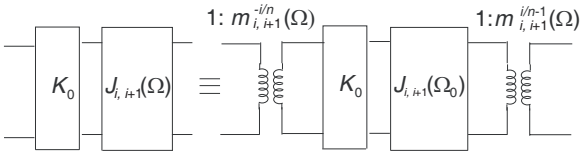

Figure 8. Decomposition of the frequency-dependent J inverters.

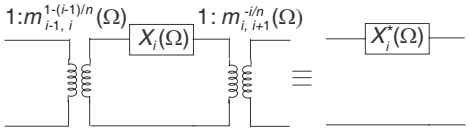

Figure 9. Turns ratio absorbed by the series reactance.

By applying the edge frequency mapping method to the quarter-wavelength resonator bandpass filters with the frequency-dependent inverter model, the mapping function can be expressed as

$$f: \begin{cases} \omega L_{ai} \to -Z_0 m_{i-1,i}^{(i-1)/n-1}(\Omega) m_{i,i+1}^{-i/n}(\Omega) \cot\left(\frac{\pi\Omega}{2\Omega_0}\right) & i = \text{odd} \\ \omega C_{ai} \to -Y_0 m_{i-1,i}^{(i-1)/n-1}(\Omega) m_{i,i+1}^{-i/n}(\Omega) \cot\left(\frac{\pi\Omega}{2\Omega_0}\right) & i = \text{even} \end{cases}. \quad (24)$$

By applying (13), we can get

$$\begin{cases} \frac{L_{ai}}{Z_0} = \frac{1}{\omega_1} m_{i-1,i}^{(i-1)/n-1}(\Omega_1) \cdot m_{i,i+1}^{-i/n}(\Omega_1) \cdot \cot\left(\frac{\pi\Omega_1}{2\Omega_0}\right) & i = \text{odd} \\ \frac{C_{ai}}{Y_0} = \frac{1}{\omega_1} m_{i-1,i}^{(i-1)/n-1}(\Omega_1) \cdot m_{i,i+1}^{-i/n}(\Omega_1) \cdot \cot\left(\frac{\pi\Omega_1}{2\Omega_0}\right) & i = \text{even} \end{cases}, \quad (25)$$

$$m_{i-1,i}^{(i-1)/n-1}(\Omega_1) m_{i,i+1}^{-i/n}(\Omega_1) \cot\left(\frac{\pi\Omega_1}{2\Omega_0}\right) \quad (26)$$

$$+ m_{i-1,i}^{(i-1)/n-1}(\Omega_2) m_{i,i+1}^{-i/n}(\Omega_2) \cot\left(\frac{\pi\Omega_1}{2\Omega_0}\right) = 0.$$

By substituting (6) with (25), the K parameters and J parameters can be calculated. It can be seen from (26) that the edge angular frequencies Ω_1 and Ω_2 satisfy different equations for different distributed resonators. This is why the bandpass filters with frequency-dependent inverters can never achieve the same ideal wide-band performance as the lumped-element bandpass prototype filter. However, if Ω_1 is fixed, the Ω_2 values calculated using (26) for every distributed resonator are very close to each other and the performance of the filters designed using this method is still very close to the ideal performance. The design example in Section 4 will show that, by using the fixed Ω_1, the bandpass filters can still achieve good equal ripple performance in a very wide bandwidth.

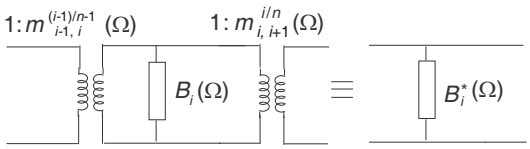

Figure 10. Turns ratio absorbed by the shunt susceptance.

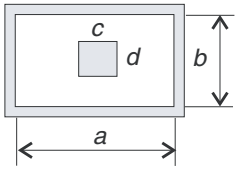

Figure 11. Cross section of the rectangular coaxial cable.

3. RECTANGULAR COAXIAL FILTERS SYNTHESIS

Rectangular coaxial cable has the advantage of low dielectric loss, low radiation loss and weak cross coupling with other circuits in a system [6]. They can be fabricated using the micromachining techniques and many applications are reported in [6–8]. Fig. 11 shows the cross section of the rectangular coaxial line. The dimensions are chosen according to [9] and [10] to make the characteristics impedance is close to 50 ohms and the cutoff frequency of the higher modes is above the frequency band of the designed filter.

3.1. Realization of *K*-inverter and *J*-inverter

In order to apply the theories in the last section to the rectangular coaxial filters synthesis, it is necessary to derive two rectangular coaxial structures as the K-inverter and J-inverter. We employed an inductive iris structure with two compensated transmission lines added on both sides as the K-inverter as shown in Fig. 12. Its equivalent model consists of a frequency-dependent K-inverter and two extra transmission lines on both sides. The extra transmission lines are added on both sides dueto the compensated transmission lines, whose phases will change with the frequency as the wavelength changes with the frequency. Fig. 13 shows the capacitive gap structure as the J-inverter and its equivalent model. The extra transmission line phase can be expressed as

$$\Delta\varphi_i(\Omega) = \varphi_i(\Omega) - \varphi_i(\Omega_0). \tag{27}$$

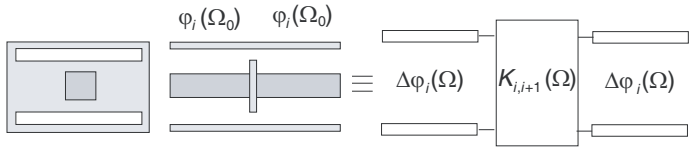

Figure 12. Realization of the K-inverter and its frequency-dependent model.

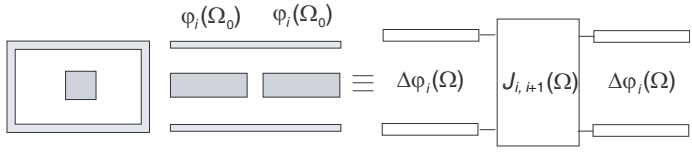

Figure 13. Realization of the J-inverter and its frequency-dependent model.

The frequency-dependent inverter can be decomposed into frequency-independent inverter with exponent-weighted turns ratio on both sides as is introduced in the last section and the extra transmission lines can be absorbed by the adjacent quarter-wavelength resonators.

3.2. Filter Synthesis

By applying the equivalent model for the inductive iris and capacitive gap structure introduced above together with the decomposition of frequency-dependent inverter in the last section, we can derive the expression for the series reactance and shunt susceptance, which absorb the turns ratio and the extra transmission lines from the adjacent inverters. They can be expressed as

$$X_i(\Omega)/Z_0 = -m_{i-1,i}^{(i-1)/n-1}(\Omega)\cdot m_{i,i+1}^{-i/n}(\Omega)$$
$$\cdot\cot\left[\frac{\pi\Omega}{2\Omega_0}+(\phi_{i-1}(\Omega)-\phi_{i-1}(\Omega_0))+(\phi_i(\Omega)-\phi_i(\Omega_0))\right]\ i=\text{odd}. \quad (28)$$
$$B_i(\Omega)/Y_0 = -m_{i-1,i}^{(i-1)/n-1}(\Omega)\cdot m_{i,\,i+1}^{-i/n}(\Omega)$$
$$\cdot\cot\left[\frac{\pi\Omega}{2\Omega_0}+(\phi_{i-1}(\Omega)-\phi_{i-1}(\Omega_0))+(\phi_i(\Omega)-\phi_i(\Omega_0))\right]\ i=\text{even}. \quad (29)$$

For derivation convenience, we take the following notations:

$$E_i(\Omega) = \begin{cases} X_i(\Omega)/Z_0 & i=\text{odd} \\ B_i(\Omega)/Y_0 & i=\text{even} \end{cases}, \quad (30)$$

$$D_i = \begin{cases} L_{ai}/Z_0 & i=\text{odd} \\ C_{ai}/Y_0 & i=\text{even} \end{cases}, \quad (31)$$

$$A_{i,\,i+1}(\Omega) = \begin{cases} K_{i,\,i+1}(\Omega)/Z_0 & i=0,2,\ldots,n \\ J_{i,\,i+1}(\Omega)/Y_0 & i=1,3,\ldots,n-1 \end{cases}. \quad (32)$$

Substitute (17) with (32), we can get

$$m_{i,\,i+1}(\Omega) = A_{i,\,i+1}(\Omega)/A_{i,\,i+1}(\Omega_0). \quad (33)$$

The mapping function for the transformation from the lowpass prototype filter in Fig. 3(a) to the bandpass filter in Fig. 6 can be written as

$$f:\omega D_i \to E_i(\Omega). \quad (34)$$

By applying (14), (28), (29) and (30), we can get

$$D_i = \frac{1}{\omega_1}\cdot\left[\frac{A_{i-1,i}(\Omega_1)}{A_{i-1,i}(\Omega_0)}\right]^{(i-1)/n-1}\cdot\left[\frac{A_{i,i+1}(\Omega_1)}{A_{i,i+1}(\Omega_0)}\right]^{-i/n}$$
$$\cdot\cot\left[\frac{\pi\Omega_1}{2\Omega_0}+(\phi_{i-1}(\Omega_1)-\phi_{i-1}(\Omega_0))+(\phi_i(\Omega_1)-\phi_i(\Omega_0))\right]. \quad (35)$$

By substituting (6) with (31) and (32), we can get

$$\begin{cases} A_{0,1}(\Omega_0) = \sqrt{\frac{D_1}{g_0 g_1}} \\ A_{i,i+1}(\Omega_0) = \sqrt{\frac{D_i D_{i+1}}{g_i g_{i+1}}}\Big|_{i=1,2,\ldots,n-1} \\ A_{n,n+1}(\Omega_0) = \sqrt{\frac{D_n}{g_n g_{n+1}}} \end{cases}. \tag{36}$$

It is noted from (35) and (36) that the calculation of parameters D_i involves parameters $A_{i,i+1}(\Omega_0)$ and the calculation of parameters $A_{i,i+1}(\Omega_0)$ involves parameters D_i. In order to solve this problem and calculate $A_{i,i+1}(\Omega_0)$, we employ an iteration procedure.

$A_{i,i+1}^{(j)}(\Omega_0)$, $A_{i,i+1}^{(j)}(\Omega_1)$, $\phi_i^{(j)}(\Omega_0)$ and $D_i^{(j)}$ are used to represent all the parameters after j iterations. The parameters after j iterations can be calculated using the parameters after $(j-1)$ iterations as

$$\begin{aligned} D_i^{(j)} = & \frac{1}{\omega_1} \cdot \left[\frac{A_{i-1,i}^{(j-1)}(\Omega_1)}{A_{i-1,i}^{(j-1)}(\Omega_0)}\right]^{(i-1)/n-1} \cdot \left[\frac{A_{i,i+1}^{(j-1)}(\Omega_1)}{A_{i,i+1}^{(j-1)}(\Omega_0)}\right]^{-i/n} \cdot \cot\left[\frac{\pi\Omega_1}{2\Omega_0}\right. \\ & \left. + \left(\phi_{i-1}^{(j-1)}(\Omega_1) - \phi_{i-1}^{(j-1)}(\Omega_0)\right) + \left(\phi_i^{(j-1)}(\Omega_1) - \phi_i^{(j-1)}(\Omega_0)\right)\right], \end{aligned} \tag{37}$$

$$\begin{cases} A_{0,1}^{(j)}(\Omega_0) = \sqrt{\frac{D_1^{(j)}}{g_0 g_1}} \\ A_{i,i+1}^{(j)}(\Omega_0) = \sqrt{\frac{D_i^{(j)} D_{i+1}^{(j)}}{g_i g_{i+1}}}\Big|_{i=1,2,\ldots,n-1} \\ A_{n,n+1}^{(j)}(\Omega_0) = \sqrt{\frac{D_n^{(j)}}{g_n g_{n+1}}} \end{cases}. \tag{38}$$

It can be seen that (37) and (38) give the calculation formulae for $D_i^{(j)}$ and $A_{i,i+1}^{(j)}(\Omega_0)$ but the formulae for $A_{i,i+1}^{(j)}(\Omega_1)$ and $\varphi_i^{(j)}(\Omega_0)$ are not provided. Actually, these two parameters can be calculated from $A_{i,i+1}^{(j)}(\Omega_0)$ using the cubic spline data interpolation functions, which will be introduced in the next part.

Since the synthesis is an iteration procedure, we should set initial parameters for the iteration. The initial parameters $A_{i,i+1}^{(0)}(\Omega_0)$, $A_{i,i+1}^{(0)}(\Omega_1)$, $\phi_i^{(0)}(\Omega_0)$ and $D_i^{(0)}$ can be calculated from the ideal inverter model. For the ideal inverter case, the exponent-weighted turns ratio and the extra transmission lines are not considered. So the calculation of $D_i^{(0)}$ is a compact form of (35) and it is written as

$$D_i^{(0)} = \frac{1}{\omega_1} \cdot \cot\left(\frac{\pi\Omega_1}{2\Omega_0}\right) = D. \tag{39}$$

Substituting (36) with (39), we can get

$$\begin{cases} A_{0,1}^{(0)}(\Omega_0) = \sqrt{\frac{D}{g_0 g_1}} \\ A_{i,i+1}^{(0)}(\Omega_0) = \frac{D}{\sqrt{g_i g_{i+1}}}\Big|_{i=1,2,\ldots,n-1} \\ A_{n,n+1}^{(0)}(\Omega_0) = \sqrt{\frac{D}{g_n g_{n+1}}} \end{cases} . \tag{40}$$

The other two initial parameters $A_{i,i+1}^{(0)}(\Omega_1)$ and $\varphi_i^{(0)}(\Omega_0)$ can be also calculated from $A_{i,i+1}^{(0)}(\Omega_0)$ using the cubic spline data interpolation method introduced in the next part.

3.3. Element Parameters Extraction

Figure 14 depicts the quarter-wavelength resonator bandpass filter realized in rectangular coaxial structures. In order to achieve the required Chebyshev response, the iris widths, gap widths and the resonator lengths must be derived.

For a given inductive iris or capacitive gap dimension, we can calculate the scattering parameters using the full-wave simulation or mode-matching program. The K parameters and the compensated transmission line phase can be derived as

$$\begin{cases} \frac{K_{i,i+1}(\Omega)}{Z_0} = \sqrt{\frac{1-|S_{11}(\Omega)_i|}{1+|S_{11}(\Omega)_i|}} \\ \phi_i(\Omega) = \frac{1}{2}(\angle S_{11}(\Omega)_i - \pi) \end{cases} , \tag{41}$$

where $S_{11}(\Omega)_i$ is the reflection coefficient of the inductive iris element. The J parameters and the compensated transmission line phase can be also calculated as

$$\begin{cases} \frac{J_{i,i+1}(\Omega)}{Y_0} = \sqrt{\frac{1-|S_{11}(\Omega)_i|}{1+|S_{11}(\Omega)_i|}} \\ \phi_i(\Omega) = \frac{1}{2}\angle S_{11}(\Omega)_i \end{cases} , \tag{42}$$

where $S_{11}(\Omega)_i$ is the reflection coefficient of the capacitive gap element.

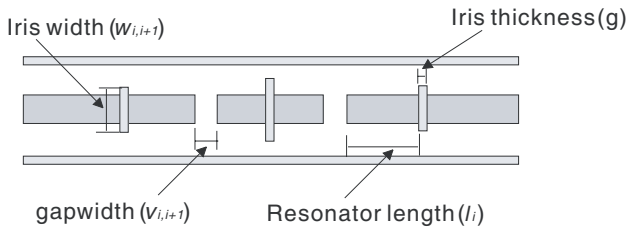

Figure 14. Configuration of the quarter-wavelength resonator bandpass filter realized in rectangular coaxial structures.

From (41) and (42) we know that it is very easy and fast to calculate the K or J parameters for the element with a given dimension by employing the full-wave simulation or mode-matching program, however, we usually need to calculate the element dimension for the required K or J parameters, which will cost much time if a search or matching program is employed.

Here we use the cubic spline data interpolation to calculate the element dimension and other parameters $A_{i,i+1}(\Omega_1)$ and $\phi_i(\Omega_0)$. First we employ a full-wave simulation to calculate the scattering parameters of the inductive iris with a series of widths $[w]$ and the capacitive gap with a series of widths $[v]$. Then the sampling data of $[K(\Omega_0)]$, $[K(\Omega_1)]$ and $[\phi_K(\Omega_0)]$ can be calculated using (41). The sampling data of $[J(\Omega_0)]$, $[J(\Omega_1)]$ and $[\phi_J(\Omega_0)]$ can be also calculated using (42). With these sampling data, we can build the cubic spline functions. The widths of the inductive iris and the capacitive gap can be calculated as

$$\begin{cases} w_{i,i+1} = S\left([K(\Omega_0)], [w], A_{i,i+1}(\Omega_0)\right) & i = 0, 2, \ldots, n \\ v_{i,i+1} = S\left([J(\Omega_0)], [v], A_{i,i+1}(\Omega_0)\right) & i = 1, 3, \ldots, n-1 \end{cases}, \tag{43}$$

where the function $S([a], [b], x)$ denotes the cubic spline interpolation function based on the sampling data $[a]$ and $[b]$ and x is the interpolation variable. The calculations of $A_{i,i+1}(\Omega_1)$ and $\varphi_i(\Omega_0)$ can be also expressed as

$$A_{i,i+1}(\Omega_1) = \begin{cases} S\left([K(\Omega_0)],\ [K(\Omega_1)],\ A_{i,i+1}(\Omega_0)\right)\ i = 0, 2, \ldots, n \\ S\left([J(\Omega_0)],\ [J(\Omega_1)],\ A_{i,i+1}(\Omega_0)\right)\ i = 1, 3, \ldots, n-1, \end{cases} \tag{44}$$

$$\varphi_i(\Omega_0) = \begin{cases} S\left([K(\Omega_0)],\ [\phi_K(\Omega_0)],\ A_{i,i+1}(\Omega_0)\right)\ i = 0, 2, \ldots, n \\ S\left([J(\Omega_0)],\ [\phi_J(\Omega_0)],\ A_{i,i+1}(\Omega_0)\right)\ i = 1, 3, \ldots, n-1, \end{cases} \tag{45}$$

After the compensated transmission line phase $\varphi_i(\Omega_0)$ is calculated, the transmission line resonator lengths are given by

$$l_i = \frac{\lambda_g(\Omega_0)}{2\pi}\left[\frac{\pi}{2} + \phi_{i-1}(\Omega_0) + \phi_i(\Omega_0)\right]. \tag{46}$$

With this approach, the element parameters extraction using the full-wave simulation is performed only one time and the sampling data can be calculated. The approach, therefore, presents a calculation procedure with the advantage that the solution is always possible and occurs rapidly.

3.4. Design Procedure

Figure 15 shows the flow diagram of the design procedure, which comprises the following steps.

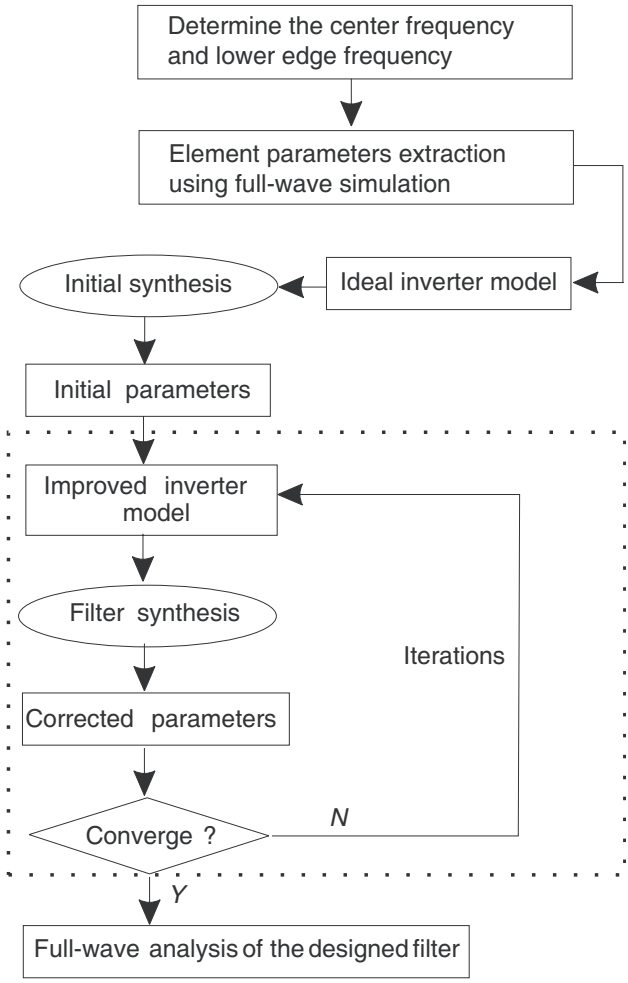

Figure 15. Flow diagram of the design procedure.

Step 1) First we should determine the center frequency and lower edge frequency according to the filter design requirement. And then different inductive iris and capacitive gap elements with a series of widths are chosen and the full-wave simulation is employed to calculate the scattering parameters at the center frequency and lower edge frequency. By applying (41) and (42), the sampling data of the K and J parameters at the center frequency and the lower edge frequency and the compensated transmission line phase are calculated.

Step 2) The ideal inverter model is employed to calculate the initial parameters $A_{i,i+1}^{(0)}(\Omega_0)$ by applying (39) and (40). The other two initial parameters $A_{i,i+1}^{(0)}(\Omega_1)$ and $\phi_i^{(0)}(\Omega_0)$ are obtained using the cubic spline data interpolation in (44) and (45) together with the sampling data in Step 1).

Step 3) Based on the initial parameters in Step 2), the improved frequency-dependent inverter model is then established. And the corrected K and J parameters at the center frequency $A_{i,i+1}^{(1)}(\Omega_0)$ are calculated according to (37) and (38). Using the cubic spline data interpolation in (44) and (45) together with the sampling data in Step 1), the other two corrected parameters $A_{i,i+1}^{(1)}(\Omega_1)$ and $\phi_i^{(1)}(\Omega_0)$ are obtained.

Step 4) A further improved inverter model is then established based on the corrected parameters. By repeating Step 3), all the parameters $A_{i,i+1}^{(j)}(\Omega_0)$, $A_{i,i+1}^{(j)}(\Omega_1)$ and $\phi_i^{(j)}(\Omega_0)$ will be further corrected.

Step 5) The Step 3) and Step 4) are repeated until the K and J parameters after N iterations $A_{i,i+1}^{(N)}(\Omega_0)$ converge. With the converged K and J parameters, the inductive iris and the capacitive gap widths and the resonator lengths are calculated using (43) and (46). Finally, a full-wave analysis of the computed filter is carried out before the designed filter is fabricated and measured.

4. DESIGN EXAMPLE AND RESULTS

The filters here are designed without global optimizations and are expected to have good in-band equal ripple performance in a wide bandwidth. Since no excessive global optimizations are needed, the time and complexity of the design procedure can be improved significantly. One example of rectangular coaxial quarter-wavelength resonator bandpass filters with a center frequency of 5 GHz is designed and presented here. The dimensions for the filter are listed in Table 1. The dimension of the rectangular coaxial cable is chosen as $a = 16$ mm, $b = 6.5$ mm, $c = 3$ mm and $d = 3$ mm.

Table 1.

g	$w_{0,1},\ w_{4,5}$	$v_{1,2},\ v_{3,4}$	$w_{2,3}$	$l_1,\ l_4$	$l_2,\ l_3$
l	1.044	0.530	4.244	7.015	9.072

The filters are designed for Chebyshev response with equal ripple performance in the passband. Because the bandwidth of the filter is very wide, the minimum passband return loss is chosen as -10 dB so that the dimension is not too small and the filter is easier to be fabricated. The designed filter is analyzed by full-wave simulations using the commercial software Ansoft HFSS [11] before it is fabricated without tuning screws. Fig. 16 shows the fabrication photo of the four-pole filter and Fig. 17 shows the measured and simulated return loss, insertion loss and group delay. It is noted from Fig. 17 that the measured results agree well with the simulation results. The passband ripple of the filter is nearly equal during the 63% fractional bandwidth (3.84–6.97 GHz). It can be also noticed from Fig. 17 that the measured insertion loss above 6.5 GHz does not agree very well with the simulated results. It may be caused by the fabrication tolerance or calibration tolerance during the measurement. In the practical applications, the filter can be designed for 20 dB return loss and the insertion loss can be improved.

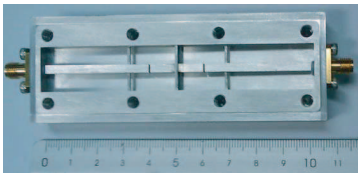

Figure 16. Fabrication photo of the designed filter.

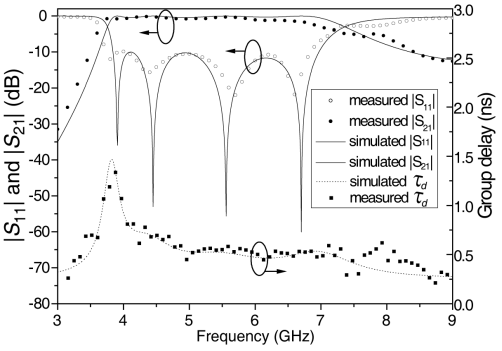

Figure 17. Simulated and measured return loss, insertion loss and group delay of the four-pole rectangular coaxial bandpass filter.

5. CONCLUSION

In this paper we have presented a dimensional synthesis method for designing wide-band quarter-wavelength resonator bandpass filters. In this synthesis method, the alternative lowpass prototype filter and the edge frequency mapping method were proposed and applied. The improved K- and J-inverter model with the exponent-weighted turns ratio was also proposed in order to incorporate the frequency

dependence of inverters. Based on the edge frequency mapping method and the improved inverter model, an iterative dimensional synthesis procedure has been presented. As design examples, a four-pole rectangular coaxial bandpass filter with 63% fractional bandwidth was designed and fabricated and the measured results agree well with the simulated results. The simulation and measurement results show good equal ripple performance in the passband. The proposed synthesis method is expected to find more applications in designing wide-band bandpass filters.

REFERENCES

1. Matthaei, G. L., L. Young, and E. M. T. Jones, *Microwave Filters, Impedance-matching Networks and Coupling Structures*, McGraw-Hill, New York, 1964.
2. Hong, J.-S. and M. J. Laucaster, *Microstrip Filter for RF/Microwave Applications*, John Wiely & Sons, 2001.
3. Levy, R., "Theory of direct coupled cavity filters," *IEEE Trans. Microwave Theory Tech.*, Vol. 15, 340–348, Jun. 1967.
4. Cohn, S. B., "Direct-coupled-resonator filters," *Proc. IRE*, Vol. 45, 187–196, Feb. 1957.
5. Matthaei, G., "Direct-coupled, band-pass with $\lambda_0/4$ resonators," *IRE National Convention Record*, Part 1, 98–111, 1958.
6. Lancaster, M. J., J. Zhou, M. Ke, Y. Wang, and K. Jiang, "Design and high performance of a micromachined K-band rectangular coaxial cable," *IEEE Trans. Microwave Theory Tech.*, Vol. 55, No. 7, Jul. 2007.
7. Llamas-Garro, I., M. J. Lancaster, and P. S. Hall, "A low loss wideband suspended coaxial transmission line," *Microw. Opt. Technol. Lett.*, Vol. 43, No. 1, 93–95, Jan. 2004.
8. Chen, R. T., E. R. Brown, and C. A. Bang, "A compact low-loss Ka-band filter using 3-dimensional micromachined integrated coax," *17th IEEE Int. MEMS Conf.*, 801–804, Maastricht, The Netherlands, Jan. 25–29, 2004.
9. Chen, T.-S., "Determination of the capacitance, inductance, and characteristics impedance of rectangular lines," *IEEE Trans. Microw. Theory Tech.*, Vol. 8, No. 5, 510–519, Sep. 1960.
10. Gruner, L., "Higher order modes in rectangular coaxial waveguides," *IEEE Trans. Microw. Theory Tech.*, Vol. 15, No. 8, 483–485, Aug. 1967.
11. ANSOFT HFSS, http://www.ansoft.com.